

Photon Emission from Si(111)-(7 × 7) Induced by Scanning Tunneling Microscopy: Atomic Scale and Material Contrast

A. Downes and M. E. Welland

Department of Engineering, University of Cambridge, Cambridge CB2 1PZ, United Kingdom

(Received 4 December 1997; revised manuscript received 5 June 1998)

Photon emission from the scanning tunneling microscope provides a signal which is dependent on the local chemical environment beneath the tip, but the details of material contrast have not been previously studied. Here we describe photon maps with material contrast, where the spatial resolution of this chemical dependent signal is a few nanometers. The resolution is governed by the size of the localized plasmon beneath the tip, which is responsible for the photon emission, and we suggest how the resolution can be made subnanometer. [S0031-9007(98)06989-0]

PACS numbers: 61.16.Ch, 73.40.Gk, 79.20.-m

Photon emission from the scanning tunneling microscope (STM) was first described in 1987 [1]. At that time, the technique promised to combine chemical information from surfaces, which is not normally possible in STM, with a resolution comparable to that of the topographic image. Subsequently, different single crystal metals have been shown to have different emission characteristics [2], but the spatial resolution of the chemical signal has not been adequately investigated. The localization of the photon emission to a small area beneath the tip promises a form of chemical microscopy, because the photon signal is related to the local chemical environment, and chemical information can be extracted from the complicated photon emission signal [3]. Understanding the confinement of this plasmon forms the basis for this Letter.

Photon emission from the STM has been found to occur for a wide variety of metal surfaces [2,4], and luminescence from semiconductors has also been investigated [5,6] as a form of local inverse photoemission spectroscopy. This technique was used on the Si(111)-(7 × 7) surface [1], but in the field emission regime for emitted photons of energy 9.5 eV, where the mechanism is dominated by the direct emission of photons by hot injected electrons. In contrast, we consider here photons in the visible range (~2.2–3.6 eV), where the mechanism of emission is the same as that for metals, i.e., the decay of localized plasmons which are excited by the tunnel current.

In our experiments, silicon (111) crystals were resistively heated in ultrahigh vacuum conditions of $<10^{-10}$ mbar. Electrochemically sharpened W tips were used, which were then cleaned and further sharpened *in situ* by Ne ion bombardment, producing typical radii of no more than a few nanometers. An in-vacuum lens, whose axis lies at 30° to the surface, accepts light at an angle of $\pm \approx 30^\circ$ or ≈ 0.7 Sr. For a vertical dipole (forced by the cylindrical symmetry) this equates to $\approx 12\%$ of the emitted light being collected, which is then focused outside the vacuum onto a photomultiplier tube used in a photon counting mode. The overall detection efficiency

(recorded counts per emitted photon) peaks at $\approx 1.6\%$ at 2.7 eV. Photon maps were recorded simultaneously with the topographic maps by counting photons for a set time at each imaging point.

Figure 1 shows a topographic and photon map collected on a Si(111)-(7 × 7) surface. In this experiment the silicon was only heated to 800 °C, so W and C contaminants still remained as the crystal was not flashed to the customary 1200 °C. The tip radius was estimated from the apparent lateral broadening of both the silicon carbide features and the monatomic steps at ≈ 30 Å, and atomic imaging was not achieved. Three distinct regions are visible in the photon map: type I regions are of silicon carbide, which are nonemitting as they are nonmetallic. These high islands are also visible in the topographic map, and pin the step flow during annealing. Type II regions are Si(111)-(7 × 7), which emit uniformly with an efficiency of 6×10^{-6} photons per tunneling electron. Type III areas exhibit narrow channels of ~ 10 nm along the lower sides of steps and triangular regions bounded by $[1\bar{1}0]$ directions. This is consistent with Si(111)-(1 × 1)-W formation which has previously been seen by ourselves and others [7,8], and the ~ 0.5 Å increase in topography matches that found in atomic imaging [8]—the W atoms originating from an earlier tip had been annealed into these monolayer islands lying on a Si(111) substrate. The efficiency in these regions is found to be 4×10^{-6} , which, despite being close to the 6×10^{-6} measured on the (7 × 7)'s, gives pronounced contrast in the photon maps. We thus have a map clearly discerning three regions: nonmetallic SiC, metallic (7 × 7)—above nonmetallic Si(111), and metallic W monolayers—also above nonmetallic Si(111). Strictly, *spectroscopy* of the emitted light is the only way to identify unknown metallic regions, but we remark that photon mapping is an ideal way of distinguishing known regions in flat surfaces. This is because all metals have different optical properties, and their emission efficiencies can vary over ~ 2 orders of magnitude.

Efficiency-voltage and efficiency-separation measurements for the 7 × 7 regions are shown in Fig. 2. The

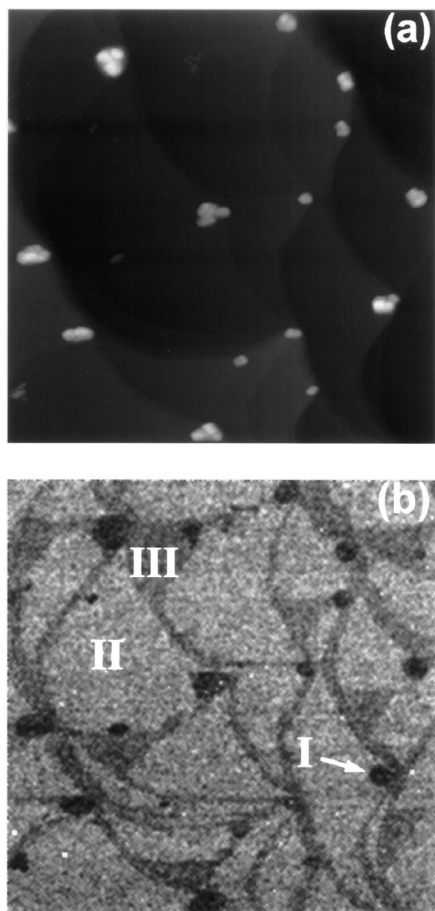


FIG. 1. (a) Topography of predominantly Si(111)-(7 × 7), with carbide structures visible. Image size: 5000 Å; height range (black-white): 133 Å; tunnel current: 10 nA; tip bias: -3.6 V. (b) Photon efficiency map of the same area. Examples of the three regions are shown [I: silicon carbide; II: Si(111)-(7 × 7); III: Si(111)-(1 × 1)-W]. Efficiencies are 6×10^{-6} emitted photons per tunneling electron (7 × 7), 4×10^{-6} [(1 × 1)-W], and below the noise level for silicon carbide. Average counts per pixel on 7 × 7 region: 32 (count rate ≈ 6 kHz). Tip radius estimated ≈ 30 Å.

efficiency-voltage curves were taken while disabling the feedback loop, which is a preferable method to maintaining the loop with a fixed current, which causes the tip-sample separation to change during the measurement. The variation in efficiency with voltage is similar to that for most metals [1,9], leveling off at ~ 4 -5 V, but the distance variation in Fig. 2(b) is in opposition to what is normally seen [10].

The optical properties of the 7 × 7 reconstruction have been measured previously [11], with an imaginary part of the dielectric function of < 10 in the optical energy range. This would suggest an efficiency lower than that for Au, but superior to that of Fe, for example, although the measured (7 × 7)'s efficiency is lower than we would expect for its optical constants. Electronically, the 7 × 7 surface is metalliclike, with a number of high density surface states as measured by STM [12], photoemission

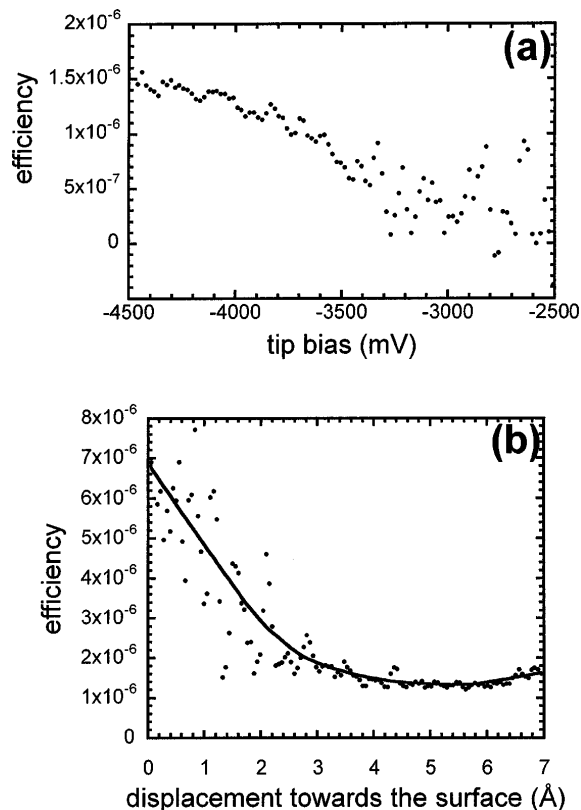


FIG. 2. (a) Photon efficiency as a function of voltage for a Si(111)-(7 × 7) region in Fig. 1. The loop was disabled with a tip bias of -2.0 V when the tunnel current was 5 nA. Below ~ -3 V the data becomes too noisy to be meaningful. (b) Efficiency as a function of displacement from tunneling (at 0 Å) towards the sample. The loop was disabled with a tip bias of -5.0 V when the tunnel current was 1 nA. The position at which the maps in Fig. 1 were taken corresponds to ~ 3 Å displacement.

[13], and inverse photoemission [1], so its measured optical properties are not surprising. The mechanism of photon emission for metallic surfaces can be thought of as starting with an excitation of a plasmon by inelastically tunneling electrons. These electrons lose energy $\hbar\omega$ to create a localized plasmon, that is, one whose position is fixed under the tip by the curved geometry. Actually, the plasmon extends into the tip, across the gap region, and decays approximately exponentially into the surface; the plasmon has an almost Gaussian shape laterally on the surface [14]. The lateral extent of the plasmon in the surface represents the resolution of a photon map across a boundary between two different metals, provided there are no topographic changes. This plasmon then either decays to a photon of the same energy or is damped out by the time response of the electrons or by losing energy to interband transitions.

We calculated the plasmon wave functions explicitly by solving Laplace's equation for a geometry of a sphere above a plane [3]. These plasmon wave functions were found to be well approximated by $\Psi \sim \exp(-x^2/2h^2)$

laterally, and $\Psi \sim \exp(-z/h)$ vertically. $h = \sqrt{Rs}$ —the geometric mean of the tip radius R and tip-sample separation s . The diameter within which 50% of the plasmon intensity is located laterally is then

$$x_0 = 2\sqrt{Rs \ln 2} \quad (1)$$

and, similarly, half the intensity in the vertical direction is located within the length

$$z_0 = \sqrt{Rs \ln 2/2}. \quad (2)$$

Both of these expressions can be termed the *resolution* of chemical mapping in each dimension. The lateral resolution of the chemical signal in Fig. 1(b) can be calculated from (1) as ≈ 2 nm for $R = 30$ Å and $s = 6$ Å. Indeed, close inspection of the image revealed material contrast over only one or possibly two pixels (2–4 nm). Contrast has previously been shown between an island of C_{60} molecules and its Au(110) substrate [15], but this may be attributed to changes in the tunnel barrier, in a similar way as to how adsorbates cause the photon signal to be reduced. The C_{60} molecules can modify the photon intensity from the surface, but the plasmon in the Au surface beneath and the properties of the emitted light (such as the ≈ 500 nm cutoff [2]) will remain unchanged, so this is not strictly material contrast.

Pseudo-atomic-resolution maps, conducted with a sharper tip and an adequately “flushed” 7×7 surface (where all contaminants are removed at 1200 °C) are presented in Figs. 3(a) and 3(b). The instabilities present are a result of requiring a high bias (3.4 V) and high current (30 nA) to produce enough counts to image faster than the thermal drift of the STM, although the surface is not damaged. The tip radius can be estimated as 10 Å from apparent step broadening, and the Ne ion cleaning process always results in an approximately spherical tip shape. We should stress that, although it is only the last atom or atoms on the end of the tip which gives rise to the tunneling current, the photon emission is dependent on the larger radius. The reduction in the emission signal from Fig. 1 (with the 3 nm radius tip) by an order of magnitude demonstrates that this 1 nm tip radius is correct, because the emission varies as R^n , where $n \approx 2.0$ – 2.5 [3]. The atomic images, and the line cuts along adatom rows in Fig. 3(c), show a contrast opposite to that found on the Au(110) surface, i.e., peaks in the photon signal coincide with the highest points of the topography in our results.

For a metallic surface, the smaller the tip-sample separation the larger the *magnitude* of the plasmon potential, so the emission efficiency should increase due to a larger dipole. This is evident from data collected from the Cu(111) surface [16], where the efficiency increases as the tip is moved towards the sample, and is also apparent in the reversed contrast from the Au(110) rows [14]. In the latter case, the tip moves vertically away from the plasmon to follow the topographic variations which are laterally smaller than the plasmon localization, and the

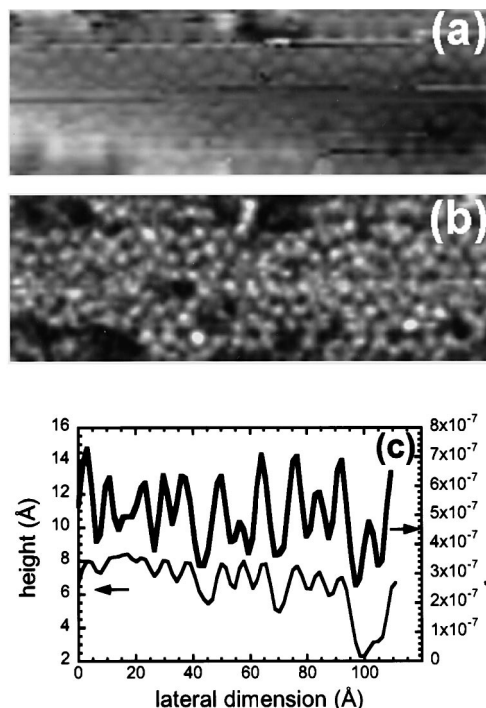


FIG. 3. (a) Topography of clean Si(111)-(7 × 7). Image size: 180 Å × 61 Å; height range: ≈ 10 Å; tunnel current: 30 nA; tip bias: -3.4 V. (b) Efficiency map of the same area, with average counts per pixel ≈ 20 . Tip radius estimated as ≈ 10 Å. (c) Line cuts of topography and efficiency taken from another part of the scan.

efficiency is reduced on top of the rows. The explanation of the opposite contrast observed in Fig. 3(c) is quite different. If the metalliclike 7×7 was continuous into the bulk, 50% of the plasmon would occur within 12 Å laterally and 2.5 Å vertically, calculated from (1) and (2) using $R = 10$ Å and $s = 5$ Å. However, the plasmon is limited to the 2 Å thick 7×7 layer above the nonmetallic bulk Si(111). When the tip is above the adatoms, the plasmon is located within this 2 Å layer, but in some positions in the unit cell the tip is directly above only the bulk (111) surface, so there is reduced efficiency. The efficiency is nonzero because the plasmon extends laterally into metallic parts of the surface, so that, when the tip is above the corner holes, a plasmon ring is formed in the surface. The convex sample curvature when the tip is above the adatoms is also likely to play a role in increasing the efficiency there [17]. The polarization of the light is expected to vary within the unit cell as the cylindrical symmetry is broken by the anisotropic distribution of the plasmon in the surface.

We now return to the efficiency-distance curves in Fig. 2(b). The depth of the plasmon is limited to 2 Å for the 7×7 surface, but not so for the Au surface. As the tip-sample separation decreases, the vertical depth of the plasmon from (2) decreases, and so the *proportion* of the plasmon unable to exist below the 2 Å deep

7×7 layer also decreases. The Au and 7×7 characteristics become increasingly similar as this 2 \AA limit becomes less important—indeed the (7×7) 's efficiency stops decreasing as the separation becomes smaller and, in fact, starts to increase as the gap becomes very small. The observed emission efficiencies in Fig. 1(b) are lower than we would expect given the optical properties of the surface because the plasmon is limited to this thin layer. The pseudoatomic maps are really a modulation of the number of atoms contributing to the photon emission from ~ 5 to ~ 10 .

In conclusion, we demonstrate material contrast from a photon emission map with a resolution of 2–4 nm, which agrees with the theoretical prediction of 2 nm when considering the plasmon localization. Variations in the photon emission at the atomic scale were then presented, and attributed primarily to the plasmon extent being limited by the finite depth of the metallic 7×7 layer. In principle, a very small radius tip ($< 1 \text{ nm}$) could produce subnanometer chemical maps of metallic surfaces, realizing the goal of photon emission—to map material contrast with a resolution comparable to topographic imaging.

This work was carried out as part of an ESPRIT basic research program (Project No. 23238, NANOWIRES).

-
- [1] J. H. Coombs, J. K. Gimzewski, B. Reihl, J. K. Sass, and R. R. Schlittler, *J. Microsc.* **152**, 325 (1988).
[2] R. Berndt, J. K. Gimzewski, and P. Johansson, *Phys. Rev. Lett.* **67**, 3796 (1991).

- [3] A. Downes and M. E. Welland, *Phys. Rev. B* **57**, 6706 (1998).
[4] R. Berndt and J. K. Gimzewski, *Int. J. Mod. Phys. B* **7**, 516 (1992).
[5] Ph. Dumas, M. Gu, C. Syrykh, A. Hallimaoui, F. Salvan, J. K. Gimzewski, and R. R. Schlittler, *J. Vac. Sci. Technol. B* **12**, 2064 (1994).
[6] J. Lindahl, M.-E. Pistol, L. Montelius, and L. Samuelson, *Appl. Phys. Lett.* **68**, 60 (1996).
[7] M. Azizan, T. A. Nguyen Tan, and R. C. Cinti, *Surf. Sci.* **178**, 17 (1986).
[8] S. M. Gray, Ph.D. thesis, University of Cambridge, United Kingdom, 1991.
[9] R. Berndt and J. K. Gimzewski, *Ann. Phys. (Leipzig)* **2**, 133 (1993).
[10] R. Berndt, J. K. Gimzewski, and P. Johansson, *Phys. Rev. Lett.* **71**, 3493 (1993).
[11] Z. Hammadi, M. Gauch, P. Müller, and G. Quentel, *Surf. Sci.* **341**, 202 (1995).
[12] R. J. Hamers, R. M. Tromp, and J. E. Demuth, *Phys. Rev. Lett.* **56**, 1972 (1986).
[13] H. Neddermeyer, U. Misse, and P. Rupieper, *Surf. Sci.* **117**, 405 (1982).
[14] R. Berndt, R. Gaisch, W. D. Schneider, J. K. Gimzewski, B. Reihl, R. R. Schlittler, and M. Tschudy, *Phys. Rev. Lett.* **74**, 102 (1995).
[15] R. Berndt, R. Gaisch, J. K. Gimzewski, B. Reihl, R. R. Schlittler, W. D. Schneider, and M. Tschudy, *Science* **2623**, 1425 (1993).
[16] R. Berndt, J. K. Gimzewski, and P. Johansson, *Phys. Rev. Lett.* **71**, 3493 (1993).
[17] R. Berndt and J. K. Gimzewski, *Phys. Rev. B* **48**, 4746 (1993).